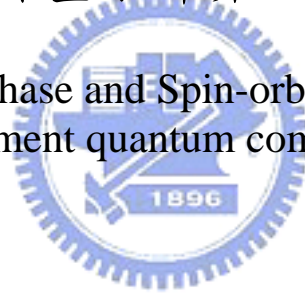# 國立交通大學

電子工程系　　　　電子研究所碩士班

碩 士 論 文

幾何相位和電子自旋軌道交互作用
用作量子計算之研究

Geometric phase and Spin-orbit interaction to
implement quantum computation

研 究 生：游清揚

指導教授：霍斯科　教授

中 華 民 國 九 十 五 年 六 月

幾何相位和電子自旋軌道交互作用
用作量子計算之研究
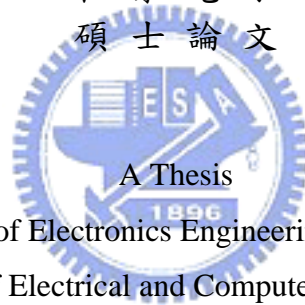# Geometric phase and Spin-orbit interaction to implement quantum computation

研 究 生：游清揚　　　　Student：Leo Yu

指導教授：霍斯科　　　　Advisor：Oleksendr Voskoboynikov

國 立 交 通 大 學
電 子 工 程 系 電 子 研 究 所
碩 士 論 文

A Thesis

Submitted to Department of Electronics Engineering and Institute of Electronics

College of Electrical and Computer Engineering

National Chiao Tung University

in partial Fulfillment of the Requirements

for the Degree of

Master

in

Electronics Engineering

June 2006

Hsinchu, Taiwan, Republic of China

中華民國九十五年六月

幾何相位和電子自旋軌道交互作用
用作量子計算之研究

學生：　　　　　　　　　　　　　　　　　指導教授：

國立交通大學
電子工程學系　電子研究所碩士班

摘　　　　要

　　在使用活動式量子位元的計算模式下，我們分別報告兩個能對實現量子計算有用的研究。在這份報告的第一個部分，我們在理論上探討了半導體對稱雙能障結構中的自旋相依穿隧效應。我們的計算是基於等效的單個能帶的 Hamiltonian 以及 Dresselhaus 自旋軌道耦合項。我們展示，帶有不同自旋方向的電子，彼此穿隧時間的比例變化可達幾個數量級。而這大且可調整的穿隧時間比例，可以作為發展全半導體的動態 spin filter 的基礎。

　　在這份報告的第二個部分，我們提出一種進行量子計算的架構，使用 ballistic electron 作為量子位元，以及耦合的量子環作為量子邏輯閘。在這個架構中，兩條相鄰且一維的量子線形成一個量子位元，它們被接到兩個互相耦合的量子環。而量子環圈繞住的奈米磁鐵提供所需的磁通量。在 Aharonov-Bohm 效應下，我們仔細設計電子波函數受到的相位調變，以促成可重新程式化且可動態控制的量子邏輯閘。基於這個架構我們可製造一組有高 fidelity 的量子邏輯閘。
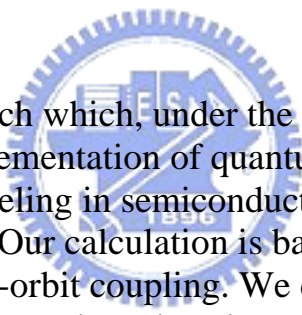
Geometric phase and Spin-orbit interaction

to implement quantum computation

student：Leo Yu   Advisors：Dr. Voskoboynikov

Department of Electronics Engineering and
Institute of Electronics
National Chiao Tung University

ABSTRACT

We present two separate research which, under the computing scheme with mobile qubits, could be useful to the implementation of quantum computation. In the first part of this report, spin dependent tunneling in semiconductor symmetric double barrier structures is studied theoretically. Our calculation is based on the effective one band Hamiltonian and Dresselhaus spin-orbit coupling. We demonstrate that the ratio of the tunneling times of electrons with opposite spin orientations can vary over a few orders in magnitude. The large and tunable ratio of the tunneling times can serve as the basis in development of all-semiconductor dynamic spin filters.

In the second part of this report, we propose an architecture to perform quantum computation, using ballistic electrons as qubits and coupled quantum rings as quantum gates. In the proposed architecture two adjacent one-dimensional wires, creating a single qubit, are connected to two coupled quantum rings, where the required magnetic flux is provided by enclosed nano-sized magnets. The phase modulation of the wave function of the ballistic electrons under the Aharonov-Bohm effect is carefully designed to facilitate re-programmable and dynamically controllable quantum gates. A set of quantum gates with high fidelity can be constructed on the basis of this architecture.

誌　　　謝

　　有句話說：作者從不可能完成一本書─他只能搞砸它。在論文必須要付梓的此刻，檢索各個研究想法的展衍，我慚愧於所完成的較之未完成的竟不及萬一。我只能希望，對於那些我應該銘謝的人而言我的謝意不嫌太早，而這研究真能開花結果的時間也不會太遲。

　　從大三下到研究所畢業的三年半時光中，指導教授霍斯科老師始終是我最主要的奧援和諮詢對象。在他擘畫的研究進程下，我能有所依循緩步前進，穩定的累積成果而獲得產出。他研究想法上的靈活多變也對我有所啟發。借居在李建平老師的實驗室中，得感謝他所經營的團隊，提供了一個較為完整的研究環境讓我得以學習成長。李老師思考上的敏銳和對待學生的大度也令我心嚮往之。

　　雖然僅僅修過朱仲夏老師一年的量子力學，但在之後的研究過程中，那不斷被證明是最核心且重要的基礎知識。在蘇正耀老師的傳習下，我才開始對量子資訊有較系統且實質的理解，特別是在關於量子纏結理論的著墨上。同時蘇老師在研究上的奉獻精神也令我景仰。感謝林聖迪老師對學生的關懷，耐心的和我討論實驗細節，甚至提出口試應該注意的地方。顏順通老師在能帶理論上的講演，增進了我對自旋軌道交互作用的理解。他在研究與教學上的認真負責也令我感佩。

　　做為實驗室兩位最資深的學長，李炳奇和林志昌學長提供了許多半導體磊晶上的知識和參考資料。他們的研究經驗傳承減少了我盲目摸索的時間。廖志豪學長在數值模擬的經驗是我很好的參考與借鑑。和黃華強學長共事的時間雖然不長，他對研究題目的親切解說緩和了我初為專題生的生澀。另外，家族學長詹前泰的論文口試水準令我嘆服，並成為我口試呈現設計概念的泉源。

　　和我同屆的實驗室同學們，宗樺、大鈞、居倫、聖偉，常常在對實驗的瞭解和設計上給我幫助，不厭其煩的詳細解說。多虧了他們的陪伴，讓我能捱過壓力最大的碩二生活。當然也不能忘了實驗室的學長和可愛的學弟妹，是它們讓我的研究生活充實且多采多姿。

我不會忘記是靠著大學同學冠成詳實的上課筆記，使我把許多心力投注於研究之餘，不致在課堂上陷入麻煩。我也必須特別感謝大學同學君浩在研究上提出實質且中肯的意見，他的問難是這篇報告進步的動力之一。感謝林彥佑同學幫我即時借到參考資料。學弟勇智和凱峻曾陪我進行一次口試預演。準備口試前夕，古道熱腸的杜宇軒學長和義氣相挺的張世鵬同學提供了許多寶貴意見。

　　在研究生涯的許多時候我無暇他顧而近乎不問世事。是因為家人們的支持和關懷，使我無後顧之憂，得以順利完成學業。還有許多值得感謝而未能一一列名於此的人，或許並不直接和這份報告相關，但對於我之成為現在的我，毋寧是更為重要的，我必須在此承認。

Contents

1

List of Figures

Chapter 1

Introduction

The idea of quantum computation can be dated back to 1982, when R. Feynman pointed out the essential difficulties in simulating quantum mechanical systems on classical computers [1]. To circumvent those difficulties he initiated to build computers based on the principles of quantum mechanics. Similar idea was proposed by Deutsch later in 1985 [2], while he sought to provide a foundation for the Church-Turing thesis based on a physical theory. The field of quantum computation and quantum information arouse widespread interest, however, not until 1994 when P. Shor demonstrated that the problem of finding the prime factors of an integer can be solved efficiently on a quantum computer [3]. It struck people like a bolt because this problem is still believed to have no efficient solution on a classical computer. Thus the finding challenges the strong Church-Turing thesis once again. Further findings signaling the power of quantum computers came in 1995, when L. Grover showed the problem of searching an unstructured database can also be sped up on a quantum computer [4]. Nowadays the competition of research toward the physical implementation of a quantum computer has become like a "gold rush".

But the impetus of this rush lends itself not only to the theoretical breakthrough on the speedup of computation. The need for ever powerful information processing capability has driven the growth of microelectronics industry over the last decades. That need can only be met by integrating more functions into even smaller chips. The resulting growth in computation power has proved to be an engineering accomplishment, so much so as to be codified as the Moore's law. Although Moore's law has approximately held true for decades since 1960s, it is not expected to be held for the next twenty years. Today the feature size of electronic devices hits the scale of nanometer, the scale where the conventional semi-classical approach ceases to be true and quantum mechanics begins to take part in. While researchers in nanoelectronics seek to exploit quantum mechanical effects to construct logic gates of the scale of few atoms, a paradigm shift to quantum computation appears to be more luring than ever.

Yet the physical implementation of a quantum computer poses a most formidable challenge. To pass the five stringent requirements for the implementation of quantum computation set by DiVincenzo et el. [6], the suitability in virtually every branch of quantum physics has been contemplated: atomic physics, quantum optics, nuclear and electron magnetic resonance spectroscopy, superconducting device physics, electron physics on liquid Helium, and mesoscopic and quantum dot research(an account of all those propositions can be found in [5]). Among the numerous schemes to implement quantum computers, solid state micro- and nano- systems draw special attention because of their obvious advantages: scalability, miniaturizability and flexibility in design. It has also been remarked that solid state physics is a most versatile branch of physics, in that almost any phenomenon possible in physics can be embodied in an appropriately designed condensed

6

matter system [6]. Naturally then, we expect the versatility of solid state systems will extend to the construction of quantum computers as well. Our later discussion indicates this proposition to be more plausible (though only time could tell if it is right).

The success of microelectronics has been built on the utilization of the charge degrees of freedom of electrons. A quantum mechanical aspect of electrons – the spin degrees of freedom – has largely been ignored. As the working dimension of semiconductor electronics devices has been reduced to such a small scale, that quantum mechanical property of electrons can no longer be neglected, the field of semiconductor "spintronics" has begun to emerge. The underlying principle of this new electronics is the intimate connection between the charge and spin degrees of freedom of electrons. Besides the possibility to enhance the performance of quantum electronic devices, the utilization of spin offers the opportunity to manipulate phase coherence over length scale much larger than is typically possible in charge-based device [6]. This is a welcoming feature especially as far as the construction of quantum computers is concerned, for spin can be a natural candidate for the qubit.

To successfully incorporate spin into existing semiconductor technology, however, one has to address technical issues such as efficient spin injection, transport control, and detection of spin polarization. A natural starting point to tackle those problems would be to pass electrons through strongly magnetized metals and then inject them back into semiconductor. But the conductivity mismatch between metal and semiconductor impedes the electron transport and makes this approach seem inefficient, as Schmidt pointed out [9]. Reported experimental results on polarization efficiency are less than 1% [10]. On the other hand, there is another approach which exploits the spin-orbit interaction in semiconductor. The spin-orbit interaction lifts the

energy degeneracy among electrons with different spin polarization, making the coherent dynamics of electron spin dependent. Based on that we can conceive ways to manipulate the transport property of the electron. We will see such an application in chapter 2.

A calculation process of a quantum computer is facilitated by distributing and exchanging quantum information among various parts of circuit. In schemes that use static qubits, this task is carried out by incorporating extra means to transport the state of the qubit. Moreover, we would need ultrafast electronics or laser pulses (on the femto second scale) to perform gate operations subcoherently (the above discussion largely follows [7]). Thus we want to use mobile qubits in solid state systems as our embodiment of qubits. If we use electrons as information carriers, there are two such choices – spin qubits and charge qubits. Quantum computing with mobile electron spins [7] is a natural extension of spintronics, its feasibility relies on our understanding of and capability in this field. In this report, therefore, we will try to address one of the elementary issues faced in spintronics rather than thoroughly discuss its capacity to implement quantum computation. Quantum computing with mobile electron charges has also been proposed recently as an attractive candidate [36, 37, 38]. Due to its relatively mature technological ground, we will look more closely at its architecture and how it can possibly be implemented in this report.

This report is organized as follows: in chapter 2, we discuss a method to carry out spin-filtering in III-V semiconductor thus obtain spin-polarized current. As described above, such method could be useful to the implementation of quantum computing as well as quantum electronics. The result of this chapter has been published in *Journal of Applied physics*, **98**, 023716. In chapter 3, we propose a novel architecture to perform quantum computation

and in particular single-qubit operations, using ballistic electrons as qubits and coupled quantum rings as quantum gates. The result of this chapter has been submitted to *Applied Physics Letters*. Finally we summarize our findings.

Chapter 2

Time resolved spin-filtering in semiconductor symmetric resonant barrier structures
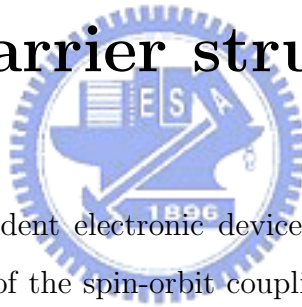
Since the first spin-dependent electronic device was proposed by Das and Datta [8], the utilization of the spin-orbit coupling has been one of the key topics of semiconductor spintronics. However, a most elementary issue, an efficient means to obtain spin polarized currents in semiconductor structures, has not been resolved yet. The inefficiency of spin-injection back from magnetized metal electrodes leads us to seek total-semiconductor alternatives. The spin-orbit interaction in semiconductors lifts the spin-degeneracy of electrons' energy, resulting in spin-dependent transport through semiconductor junctions, which thus provides a possible solution.

The spin-orbit interaction of electrons in III-V semiconductor materials is usually described by two contributions to the effective one-band spin-dependent Hamiltonian. One, often referred to as the Rashba term, is induced by the inversion asymmetry of the macroscopic potential [11], which

10

can be controlled by an external electric field or material growth techniques. The other, referred to as the Dresselhaus term [12], is due to the inversion asymmetry of the zinc-blende lattice. The interplay between these two terms has been studied by de Andrada e Silva [13], showing that, for narrow gap semiconductors, the contribution from the Rashba term to the spin-orbit interaction dominates over that from the Dresselhaus term. Hence the Dresselhaus term is often neglected. Calculations based on the Rashba spin-orbit interaction in III-V semiconductor heterostructures have been performed [14, 15, 16, 17, 18, 19], showing the all semiconductor tunneling structures can be a feasible means to obtain electronic spin-polarized currents. However, it was suggested recently [20, 18, 21] that even through a single symmetric barrier, where the contribution from the Rashba term cancels out due to macroscopic symmetry [14], electrons can tunnel highly spin-polarized because of the Dresselhaus term.
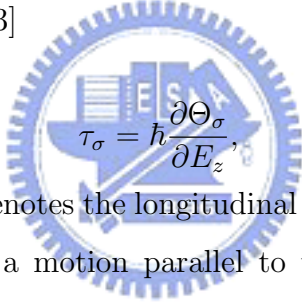
In this paper we elaborate on this idea and evaluate the spin-dependent tunneling (delay) time in a symmetric resonant tunneling structure. The tunneling time is an important quantity in a tunneling process that determines the dynamic working range of tunneling devices. In this work we take the "stationary phase approach" to define the tunneling time, as taken by Bohm [22, 23]. Our following discussion will reveal that when the spin-orbit interaction effect comes into play, the ratio of the tunneling time between differently spin-polarized electrons can gain a few orders of magnitude. This provides the theoretical basis for time-resolved spin-filtering. We also suggest that one can manipulate the tunneling time to a great variety by changing the barrier width. The relation between the delay time and the width is simple and can be used as a rule to select working frequencies.

This chapter is organized as follows. In Sec. 1 we detail our calcula-

tion of the electron spin-dependent transmission amplitude, of polarization efficiency, and of tunneling time. In Sec. 2, results of calculations for In-GaAs/InAlAs/InGaAs double barrier tunnel structure are presented. In Sec. 3 we summarize the results.

2.1   Polarization efficiency and tunneling time

We consider the spin-dependent tunneling process through a symmetric double barrier structure grown along $z||[001]$ direction, as shown in Fig. 2.1(a). Taking the "stationary phase approach" the tunneling time is described to be the phase delay time, which is the energy derivative of the phase Θ of the transmission amplitude [23]

$$\tau_\sigma = \hbar \frac{\partial \Theta_\sigma}{\partial E_z},$$

(2.1)

where $\Theta_\pm = \arg |t_\pm|$, E_z denotes the longitudinal component of the electron's energy (corresponding to a motion parallel to the heterostructure growth direction), and $\sigma = \pm 1$ refers to the spin polarization.

Our calculation is performed on the base of the effective electronic one band Hamiltonian, energy- and position- dependent electron effective mass approximation and the Ben Daniel-Duke boundary conditions [24]. Layers of the structure are perpendicular to the z-axis, the in-plane electron's wave vector is $\mathbf{k}$. With the above assumptions the electronic wave function in the jth region can be presented as

$$\Phi_\sigma(x, y, z) = \Psi_{j\sigma}(z)\exp(i(k_x x + k_y y)),$$

(2.2)

where $k = \sqrt{k_x^2 + k_y^2}$ and $\Psi_{j\sigma}(z)$ satisfies the z-component of the Schrödinger equation

$$\hat{H}_{j\sigma}\Psi_{j\sigma}(z) = E\Psi_{j\sigma}(z)$$

(2.3)

12
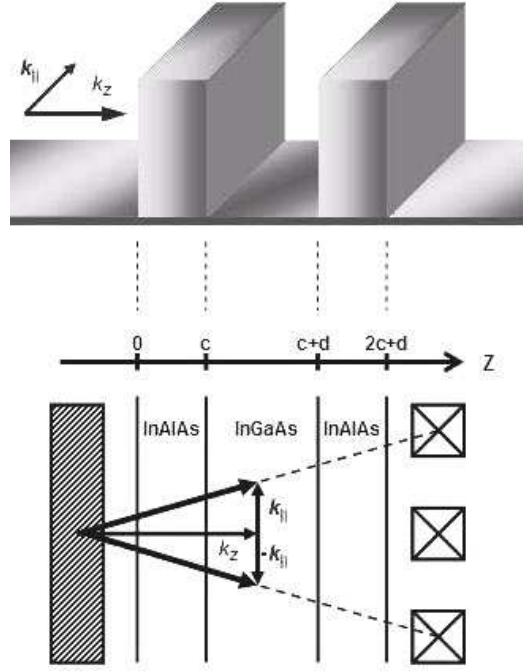
Figure 2.1: (a) Sketch of electron tunneling with the wave vector $(\mathbf{k}, k_z)$, where $\mathbf{k}$ is the in-plane wave vector and $z \parallel [001]$ - direction of the structure growth. The variation of the band parameters forms a symmetric double barrier tunneling heterostructure. (b) A schematic illustration of a possible spin-filter implementation.

with the spin-dependent Hamiltonian in each region [20]

$$\hat{H}_{j\sigma} = \hat{H}_{j0} + \hat{H}_{jSO}. \tag{2.4}$$

In Eq. (2.4) H_{j0} is the Hamiltonian of the system without spin-orbit interaction

$$\hat{H}_{j0} = -\frac{\hbar^2}{2m_j(E)} \left(\frac{d^2}{dz^2} - k^2 \right) + E_{jc},$$

and

$$\frac{1}{m_j(E)} = \frac{2P^2}{3\hbar^2} \left[\frac{2}{E - E_{jc} + E_{jg}} + \frac{1}{E - E_{jc} + E_{jg} + \Delta_j} \right], \tag{2.5}$$

13

presents the energy and position dependent reciprocal effective mass. E_{jc}, E_{jg} and Δ_j stand for the position dependent conduction-band edge, band gap and the spin-orbit splitting in the valence band. P is the momentum matrix element [24]. In Eq. (2.4) $\hat{H}_{jSO}$ is the spin-dependent part of the Hamiltonian which originates from the Dresselhaus term (in the symmetrical structure the Rashba spin-orbit coupling vanishes [14]). When the kinetic energy of electrons is substantially smaller than the barrier's height we can present this term as the following [20]

$$\hat{H}_{jSO} = \gamma_j(\hat{\sigma}_x k_x - \hat{\sigma}_y k_y)\frac{d^2}{dz^2}, \qquad (2.6)$$

where $\hat{\sigma}_x$ and $\hat{\sigma}_y$ are correspondingly x and y components of the vector of the Pauli matrices $\hat{\sigma} = \{\hat{\sigma}_x, \hat{\sigma}_y, \hat{\sigma}_z\}$ and γ_j is a material constant of the jth region.

The boundary conditions for the solution $\Psi_{j\sigma}(z)$ at the interface between j and $j+1$ regions have been introduced in Ref.[24]

$$\frac{1}{m_j(E)}\left\{\frac{d}{dz}\Psi_{j\sigma}(z)\right\}_{z=z_j} = \frac{1}{m_{j+1}(E)}\left\{\frac{d}{dz}\Psi_{j+1\sigma}(z)\right\}_{z=z_j},$$

$$\Psi_{j\sigma}(z_j) = \Psi_{j+1\sigma}(z_j). \qquad (2.7)$$

To diagonalize the Hamiltonian one can put the in-plane wave-vector $\mathbf{k}$ along the x-direction ($k_y = 0$) and take the electronic wave functions to be

$$\Psi_{j\pm}(z) = \psi_{j\pm}(z)\begin{pmatrix} 1 \\ \mp 1 \end{pmatrix},$$

which are eigenfuctions of $\hat{\sigma}_x$.

The general solution of Eq. (2.3) in a given jth region has the form

$$\psi_{j\sigma}(z) = a_{j\sigma}\phi_{j\sigma}^+(z) + b_{j\sigma}\phi_{j\sigma}^-(z),$$

where $\phi_{j\sigma}^{\pm}(z)$ is a pair of linearly independent solutions of Eq. (2.3) within that region. In the regions $j = 1, 3, 5$ the solutions are the following plane wave sets

$$\phi_{j\sigma}^{\pm}(z) = \exp(\pm ik_j z),$$

where

$$k_j(E_z, k) = \frac{\Sigma_{j\sigma}}{\hbar} \sqrt{2m_j(E_z, k)(E_z + E_{1c} - E_{jc}) - \hbar^2 \left[1 - \frac{m_j(E_z, k)}{m_1(E_z, k)}\right] k^2},$$

$$\Sigma_{j\sigma} = \sqrt{1 + \sigma \frac{2\gamma_j m_j(E_z, k)}{\hbar^2} k},$$

and E_z is the longitudinal component of the total energy in the first region:

$$E = E_{1c} + E_z + \frac{\hbar^2 k^2}{2m_1(E_z, k)}.$$

We use this expression, along with Eq. (2.5), to find the dependence of $m_j(E_z, k)$ on $E(E_z, k)(j = 1 - 5)$. In the regions $j = 2, 4$, the solutions are chosen to be

$$\phi_{j\sigma}^{\pm}(z) = \exp(\pm q_j z),$$

where

$$q_j(E_z, k) = \frac{\Sigma_{j\sigma}}{\hbar} \sqrt{2m_j(E_z, k)(E_{jc} - E_{1c} - E_z) + \hbar^2 \left[1 - \frac{m_2(E_z, k)}{m_1(E_z, k)}\right] k^2}.$$

The coefficients $\{a_{j\sigma}, b_{j\sigma}\}$ are to be determined from the boundary conditions, Eq. (2.7). The sets of coefficient in neighboring regions are related by the transfer matrix M [25]:

$$\begin{pmatrix} a_{j\sigma} \\ b_{j\sigma} \end{pmatrix} = M_\sigma^j \begin{pmatrix} a_{j+1\sigma} \\ b_{j+1\sigma} \end{pmatrix}$$

According to the boundary conditions Eq. 2.7 the matrix M_σ^j is written as [14]

$$M_\sigma^j = \frac{1}{\Delta_j} \begin{pmatrix} \Lambda_{j+}^- & \Lambda_{j+}^+ \\ -\Lambda_{j-}^- & -\Lambda_{j-}^- \end{pmatrix}$$

with

$$\Delta_j = \Delta_j^+ - \Delta_j^-, \quad \Delta_j^\pm = \left\{ \frac{d}{dz} \ln[\psi_{j\sigma}^\pm(z)] \right\}_{z=z_j},$$

$$\Lambda_{j+}^\pm = \left(\frac{m_j}{m_{j+1}} \Delta_j^\pm - \Delta_j^+ \right) \frac{\psi_{j+1\sigma}^\mp(z_j)}{\psi_{j\sigma}^+(z_j)},$$

$$\Lambda_{j-}^\pm = \left(\frac{m_j}{m_{j+1}} \Delta_j^\pm - \Delta_j^- \right) \frac{\psi_{j+1\sigma}^\mp(z_j)}{\psi_{j\sigma}^+(z_j)}.$$

The double barrier tunneling structure consists of four interfaces, so the total transfer matrix is written as

$$M_\sigma = \prod_{j=1}^{4} M_\sigma^j.$$

Electrons are injected from the region $j = 1$. The transmitted waves will appear in the region $j = 5$. With this assumption the transmission amplitude is given by

$$t_\sigma = \frac{1}{(M_\sigma)_{11}},$$

and the spin-dependent delay time is written as

$$\tau_\sigma(E_z, k) = -\hbar \frac{\partial \arg\left[(M_\sigma)_{11}\right]}{\partial E_z}.$$

The polarization efficiency of the structure was defined in [14] to be

$$P = \frac{|t_+|^2 - |t_-|^2}{|t_+|^2 + |t_-|^2}.$$

16
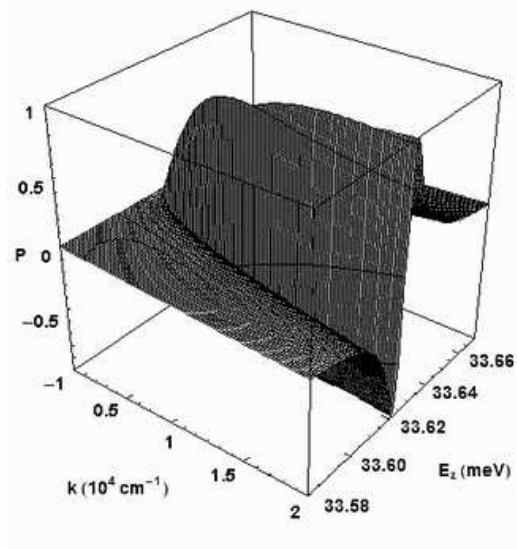
Figure 2.2: Polarization efficiency P calculated for a $In_{0.53}Ga_{0.47}As/In_{0.52}Al_{0.48}As/In_{0.53}Ga_{0.47}As$ DBT structure (see Fig. 2.1). The structure parameters are obtained in Refs. [27]: $E_{1g} = 0.418$ eV, $E_{2g} = 1.52$ eV, $\Delta_1 = 0.38$ eV, $\Delta_2 = 0.341$ eV, $m_1(0) = 0.044\ m_0$, $m_2(0) = 0.084\ m_0$ (m_0 is the free electron mass), $\gamma_1 = 0.0769$ eV nm^3 [20], $\gamma_2 = 0.0734$ eV nm^3 [28], $c = 6$ nm, $d = 12$ nm.

2.2 Calculation results

In Fig. 2.2 we demonstrate the numerical results of the polarization efficiency P of an electron's tunneling through a resonant symmetric structure made of $In_{0.53}Ga_{0.47}As$ /$In_{0.52}Al_{0.48}As$ heterojunctions. All calculations are performed within a region on (E_z, k) plane where the total energy of electrons is substantially smaller than the barrier's height (see Eq. 2.6). The numerical values of γ in different materials are obtained for InAs and GaAs from Ref. [20], for AlAs from Ref. [28], for alloys with the Vegard's superposition law [29]. One can see that the polarization efficiency shows typical resonant behaviors as a function of the longitudinal energy and in-plane wave-number.

The peaks correspond to the spin-split lowest resonant levels on the (E_z, k) plane. The splitting of the resonant levels result in an abrupt change of the sign of the polarization efficiency.
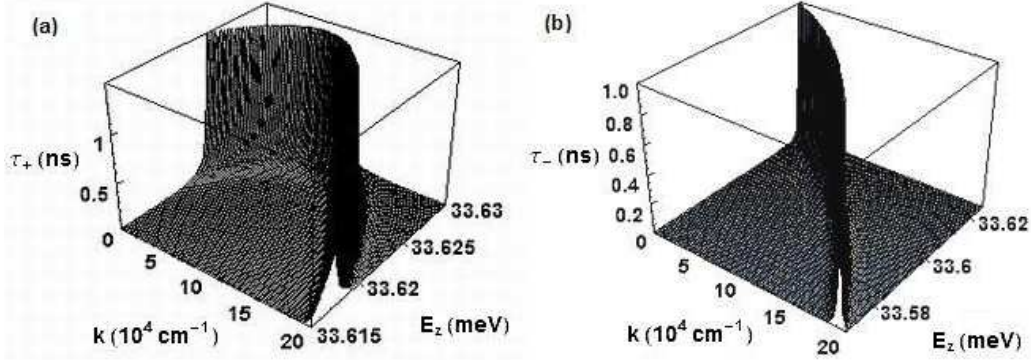
Figure 2.3: The delay time for the structure in Fig. 2.2. (a) Delay time for electrons with spin "up". (b) Delay time for electrons with spin "down".

The delay time of tunneling electrons with two opposite spin polarization is presented in Fig. 2.3. The position of the peak corresponds to the resonant tunneling level, at which the tunneling electron is "trapped" in the quasi-bound states of the well. Although the positions of the peak for the two opposite spin polarizations do not seem to have the same functional dependence on (E_z, k), the distance between them in E_z is proportional to k, in accordance to the linear dependence on k of the Dresselhaus spin-spliting of the levels in the well.

Since the positions of the peaks depends sharply on E_z and k, we present in a logarithmic scale the ratio of the delay time between oppositely spin-polarized electrons (see Fig. 2.4). This ratio increases with the length of k-vector and can gain a few orders in magnitude.

The ratio of delay times can be tuned by means of structural design. For this reason we present in Fig. 2.5 the dependence of the maximal delay time

18
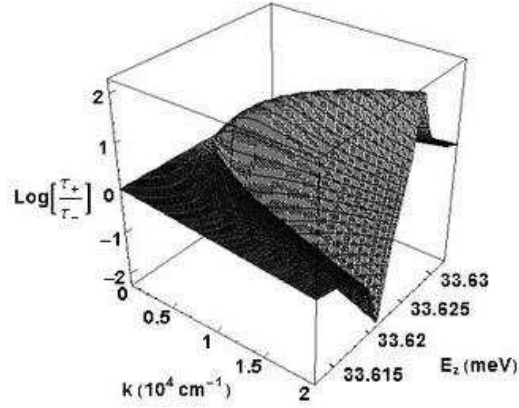
Figure 2.4: Ratio between the delay time for different polarizations of the electron spin. The structure is the same as in Fig. 2.2.

on the barrier thickness c and the well width d. The delay time increases with the increasing of c and d, but has different functional dependencies on each of them. From the calculation results presented in Fig. 2.5 for τ_+, one can approximate the dependencies as the following formula:

$$\tau_+ \propto d^2 \exp(\alpha c),$$

α is a constant; for τ_- of the same structure, one can recalculate it from the logarithmic ratio. For our symmetric InGaAs/InAlAs/InGaAs double barrier structure $\alpha \approx 0.074$ when $d = 18nm$. Applying this formula one can determine the actual region of frequencies where the structure is applicable to spin-dependent electronic devices.

The large and tunable ratio of spin-dependent delay times in symmetric structures provides a new method to perform spin-filtering. Once we have clearly spin-distinguishable times of the tunneling processes, the cutoff frequencies of electrons differently spin-polarized will also split. By selecting an appropriate region of frequency, the current contribution from electrons with lower cutoff frequency can be greatly suppressed. In this sense we achieved

19
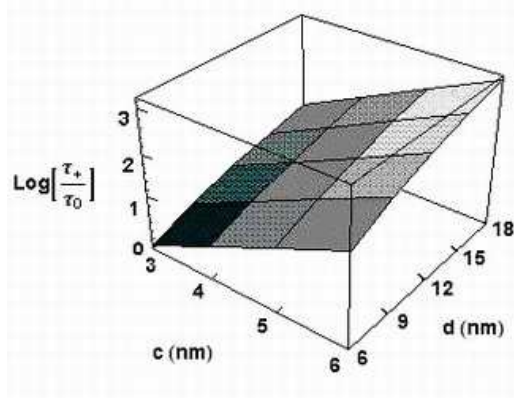
Figure 2.5: The variation of the maximum delay time with respect to (a) the barrier thickness. (b) the well width. The constant $\tau_0 = 10^{-12}$ s is defined for normalization. The structure is the same as in Fig. 2.2.

time-resolved spin-filtering. This dynamic regime is more efficient than the conventional static regime. Indeed, in the static regime the means to spin-filtering is a large spin-splitting of resonant levels in the well [16], which requires a large transversal DC bias (or built-in electric field). In symmetrical structures instead one can perform the dynamic spin-filtering even when only a weak time dependent signal is applied. We mention by pass that the spin-relaxation processes can also be suppressed by the same means.
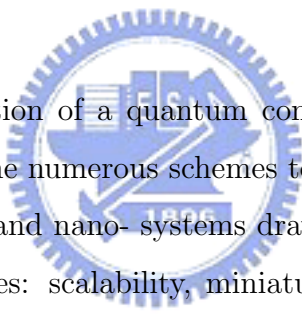
An important point tends to be missed is that the spin-filtering based on the spin-orbit coupling requires a control of electrons' in-plane momentum [16, 18, 19]. Fig. 2.1(b) illustrates schematically the basic concept of a dynamic spin-filter fabricated in a split multi-collector configuration. The in-plane momentum control of electrons and the dynamic spin-filtering are achieved by sending a series of high frequency voltage pulses to different leads of the multi collector. Another method to control electrons' in-plane momentum was demonstrated recently with side-gated resonant devices in a DC regime [19].

20

2.3 Conclusions

Based on the stationary phase concept and the effective one-band Hamiltonian with the Dresselhaus spin-orbit coupling, we present the numerical results of the tunneling time through a realistic InGaAs/InAlAs/InGaAs resonant symmetric structure. It is shown that the polarization efficiency of the structure has a well-defined resonance behavior, which leads to a considerable spin polarization of electrons tunneling through. In the lower energy region, the ratio between the tunneling times of electrons with opposite spin orientation can vary over a few orders in magnitude. The results indicate that the Dresselhaus spin-orbit coupling separates the time-dependent response of differently spin-polarized tunneling electrons. Further, the large and tunable ratio of the tunneling times provides a possible way to construct a dynamic spin filter. The characteristic time of such devices also has been estimated and presented, showing simple functional dependencies on the barrier thickness and the well width. The dependencies can be exploited to design spintronic devices working in the desired frequencies.

Chapter 3

Aharonov-Bohm quantum gates with ballistic electrons

The physical implementation of a quantum computer continues to pose a great challenge. Among the numerous schemes to implement quantum computers, solid state micro- and nano- systems draw special attention because of their obvious advantages: scalability, miniaturizability and flexibility in design. Quantum computation using ballistic electrons has been proposed recently as an attractive candidate [36, 37, 38]. In this scheme we use ballistic electrons as flying qubits in one dimensional quantum wires within the dual rail representation [38, 44]. That is, two adjacent 1D quantum wires, called the **0-** and the **1-**rail respectively, are used as the physical implementation of a single qubit. The logic state $|0\rangle$ is defined as the presence of a single electron in the **0-**rail while the logic state $|1\rangle$ as in the **1-**rail. Initialization and measurement of the qubit states are done by coupling each qubit rail to a single electron transistor, as was proposed in [38]. The construction of quantum gates deserves more discussion so from hereon we pay special attention to it.

After the first idea of utilizing quantum interference effects to perform logic functions has been proposed by Datta et el. [40], the property of quantum waveguide and quantum network has been widely investigated. Among them are quantum interference transistors [40, 47], serial stubs [30] and Ahanorov-Bohm rings with multiple arms [31], to list only a few. A complete set of logic functional devices has also been proposed by Wu. et el. [45], leading to the possibility of performing massive parallel computing by electron wave. Those previous works, however, focus mainly on the manipulation of transmission probability but not on the accompanying changes on the phase of the wave. That is, they concentrated on the possibility to perform classical computation but miss the even more natural application to perform quantum computation. Thus we are motivated to explore the capacity of quantum interference devices to perform single-qubit operation in the context of quantum computation using ballistic electrons. But to achieve that end we would like to look at the existing quantum network theory in a new setting first.

3.1 A detour to microwave engineering

In this detour we will first provide an equivalent description of the quantum network, which brings us more flexibilities in designing the quantum network and gives insight into the capacity of quantum interference devices. Then we adopt those ideas to create a single-qubit quantum gate for ballistic electrons. All knowledge about microwave engineering used in this section can be found in [34].

It is well-known that both the time-independent Schrödinger equation and the the source-free Maxwell equations take the form of the Helmholtz

equations. Further resemblance appears when we consider the TEM solutions of the Maxwell equations in waveguides, i. e., the transmission line equation [34], and the one-dimensional Schrödinger equation in constant potential. The analogy can be most directly seen as follows: In the transmission line theory we concern only two integrated physical quantities of the electric circuit, the electrical potential $V(x)$ and the electrical current $I(x)$, but not the detailed field solutions of the Maxwell equations. Their solutions in a lossless transmission line are:

$$
\begin{aligned}
V(x) &= V_0^+ e^{i\beta x} + V_0^- e^{-i\beta x}, \\
I(x) &= \frac{V_0^+}{Z_0} e^{i\beta x} - \frac{V_0^-}{Z_0} e^{-i\beta x},
\end{aligned}
$$

where Z_0 is the characteristic impedance of the transmission line and β is the propagation constant. However, in constant potential the time-independent one-dimensional Schrödinger equation has solutions:

$$
\begin{aligned}
\psi(x) &= a_1 e^{ikx} + a_2 e^{-ikx}, \\
\frac{\partial \psi(x)}{\partial x} &= a_1 ik e^{ikx} - a_2 ik e^{-ikx},
\end{aligned}
$$

and $k = \frac{\sqrt{2m^*(E-V)}}{\hbar}$, V is a constant potential. If we regard ik as a wave conductance in the quantum network as $\frac{1}{Z_0}$ in the transmission line, those two sets of solutions take the same form. Their boundary conditions are also the same. In the transmission line equation we require the continuity of the voltage $V(x)$ and the conservation of the current $I(x)$ at each intersection; in a one-dimensional quantum network we require the continuity of the wave function $\psi(x)$ and the conservation of the current $\frac{\partial \psi(x)}{\partial x}$ by the Griffiths boundary conditions [35, 47]. Thus we can draw freely the already sophisti-

24

cated circuits and techniques from the microwave engineering to apply to a quantum network.

Then we immediately see that a quantum interference transistor in [47] amounts to a single stub. Total transmission occurs (see Fig.7 in that reference) when $kL/\pi = \frac{n}{2}$, $n \in \mathbb{Z}$, or $L = \frac{n\lambda}{4}$, i.e., when the single stub acts as a quarter-wave transformer such that the infinite load is transformed into a zero load. An impurity introduced into the quantum network, modeled as a δ-function in [33], is like a conductance connected in series. It can be put at the intersection of multiple segments of 1D quantum wires to match the wave impendence of the quantum network. The inclusion of external magnetic field breaks the reciprocity of the quantum network, creating anisotropic quantum interference devices. These devices include the isolator and the quantum circulator, both of which prevent reflected waves of the next stage from further interfering with the input waves. All the above mentioned structures give us more flexibilities in designing quantum network to do computation.

Having seen a variety of quantum interference devices, we now want to make use of them to perform single-qubit operation. Again let's look at some of the existing microwave circuits first. The (180°) hybrid works as a Hadmard gate. The quadrature(90°) hybrid (see the figure below) is especially interesting. Let the input and output electron have a wave number
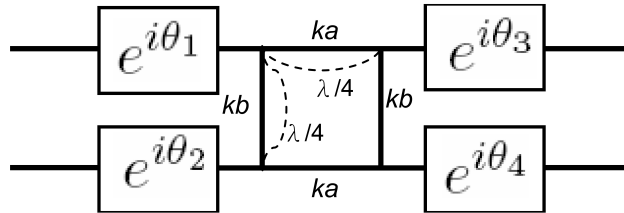
$k = \sqrt{2m^*E}/\hbar$, where E stands for the electron energy and m^* for the electron effective mass. Also, let ka and kb be the electron wave number in the corresponding segments of 1D quantum wires in Fig. 3.1. The length of each

of the four internal segments of 1D quantum wires is chosen to be $\frac{\lambda}{4}$ with respect to the corresponding wave number in that segment. Connecting four phase shifters [38] to it, the transfer matrix of this quadrature(90°) hybrid would be

$$\begin{pmatrix} \sqrt{\frac{\alpha}{\alpha+1}}e^{i(\theta_1+\theta_3)} & -i\sqrt{\frac{1}{\alpha+1}}e^{i(\theta_2+\theta_3)} \\ -i\sqrt{\frac{1}{\alpha+1}}e^{i(\theta_1+\theta_4)} & \sqrt{\frac{\alpha}{\alpha+1}}e^{i(\theta_2+\theta_4)} \end{pmatrix},$$

where $\alpha = ka/kb$. By controlling over α and θ_i, $i = 1 - 4$, this configuration can be constructed to act as arbitrary single-qubit quantum gate.

There are two problems with this construction, however. To have an identity or a σ_x gate, α has to approach to infinity or zero. This is impractical for α is related to the voltage applied to different segments of 1D quantum wires. The second problem arises since we require the length of each of the four internal segments of 1D quantum wires to be $\frac{\lambda}{4}$ with respect to the corresponding wave number in that segment. Different ka and kb require different length for the corresponding segments. If we have no means to vary the length of each segment of quantum wire, then the functionality of such quantum gates could not be changed after fabrication.

The ability to construct quantum gates by total electrical means is not all satisfying. Adding an external magnetic field to electric circuits, however, can further modulate the phases of the electronic waves of the ballistic electrons (the Aharonov-Bohm (AB) effect [39, 40]). So, we propose in this chapter a system of one-dimensional (1D) quantum wires incorporating an array of nano-rings and nano-sized magnets [43] which can act as a new architecture to perform quantum computation. Each quantum gate in this architecture is controlled dynamically by flipping the magnetization of the nano-sized magnets and changing the chemical potential for the ballistic electrons. This provides the opportunity to program dynamically a quantum computer the

same way as we do a classical one.

3.2 General architecture

Our architecture is shown conceptually in Fig. 3.1. A pair of adjacent quantum rings, which enclose nano-sized magnets (represented in Fig. 3.1 as tablets with arrows) stands for a single-qubit AB quantum gate (basic element). Figure 3.1 shows two single qubit gates and a controlled phase shifter [38]. The phase shifter enables the entangling of two single qubits and to form a two qubit gate. During a quantum computation cycle, two input qubits enter from the two pairs of parallel 1D quantum wires at the left-hand side (the rails) two AB quantum gates. Their wave functions interfere and become modulated under the AB effect in the quantum rings, then they leave and enter finally the two pairs of parallel 1D quantum wires at the right-hand side. Note that the two pairs of quantum wires at the left-hand side are separated far enough to minimize the Coulomb interaction between different qubits. After two single-qubit operations (being performed in two separated pairs of quantum rings), rails leaving the AB quantum gates enter path selectors, which could either direct electrons to a position close enough to "turn on" the Coulomb interaction between them (for instance, the lightly shaded region in Fig. 3.1), or lead electrons away from the interaction region (then "turn off" the interaction). Path selectors can be realized by making the potential barrier on a certain path high enough or by a quantum circulator [45]. With a carefully designed length of the interaction region, the two qubits altogether will undergo a controlled phase shift transformation [38]. Since single- and two-qubit gates can be implemented, our architecture is scalable and can be expanded to perform arbitrary multi-qubit quantum
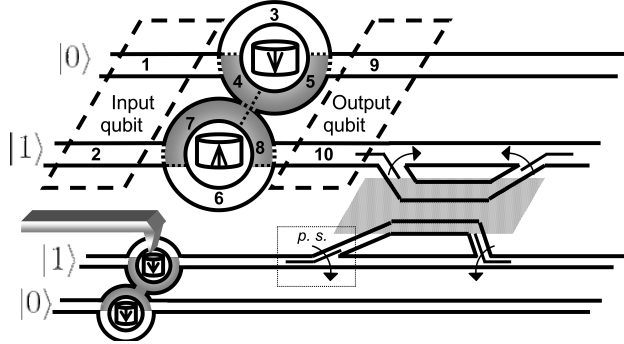
Figure 3.1: Schematic diagram of the proposed architecture for quantum computation. Two pairs of parallel 1D quantum wires represent two qubits connected to two pairs of quantum rings, each of which stands for a single-qubit quantum gate. The tablets in the rings are single-domain nano-sized magnets (the arrows indicate their magnetization), and the cantilever is used as a read-write head to monitor/control the magnetization. Path selectors (abbreviated as p.s.) are used to lead electrons to/away from the lightly shaded region (phase shifter), where the Coulomb interaction between electrons is strong enough to entangle two qubits. The numbers in the upper-left corner indicate the segments of the 1D quantum wires used in the calculation of a single-qubit gate.

computations [46]. From now on we focus on the construction of the single-qubit AB quantum gate in our discussion.

3.3 Calculation and results

To determine the operations that a single qubit undergoes by passing the AB quantum gate, we evaluate the transmission matrix $\mathbf{T}$ between the input and output of the gate (see the upper-left corner of Fig. 3.1). Assuming the single-modedness in each segment j of 1D quantum wave guides , we

adopt the method proposed in [47], where the electron wave functions are represented by 1D plane waves. In the input and output leads (segments $j = 1, 2, 9, 10$ in Fig. 3.1) the electron wave vector is $k = \sqrt{2m^*E}/\hbar$, where E stands for the electron energy and m^* for the electron effective mass. The wave numbers of the plane wave solutions in the jth segment of quantum wire (for $j = 3, 6$) are chosen to be $k_{i\pm} = k \pm \pi\phi_i/L$. Here the normalized flux ϕ is defined by $\phi_i = \Phi_i/\Phi_0$, where Φ_i is the magnetic flux through the upper ($i = 1$) or lower ($i = 2$) ring. $2L$ stands for the circumference of a quantum ring and " $\pm$ " indicates whether the electron wave vector has the same direction as the magnetic vector potential or not. $\Phi_0 = \hbar/e$ is the universal flux quantum. In the segments $j = 4, 5, 7, 8$ the electron wave number is given by $k_{i\pm} = k_g \pm \pi\phi_i/L$. The wave number k_g can differ from k and depends on changes in the chemical potential or the shape of the segment. Applying standard techniques one can calculate the matrix elements T_{nm} of the transmission matrix, which relates the input and output electronic wave functions as

$$\begin{aligned}
|0\rangle_{out} &= T_{11}|0\rangle_{in} + T_{12}|1\rangle_{in} \\
|1\rangle_{out} &= T_{21}|0\rangle_{in} + T_{22}|1\rangle_{in}.
\end{aligned}$$

State $|0\rangle$ or $|1\rangle$ is the electronic wave propagating in the upper or lower rail correspondingly.

The quantum gate represented by the transmission matrix $\mathbf{T}$ is in general not unitary. However, we stress that with properly configured gates the transmission rate is sufficiently high to perform a reasonably long quantum computation. The probabilities of transmission T_0 from the input **0**-rail to the upper and T_1 to the lower output rail for a particular k_g/k are shown in Fig. 3.2 ($\mathrm{T}_0 = |T_{11}|^2$, $\mathrm{T}_1 = |T_{12}|^2$). The transmission probabilities are periodic functions of kL/π and ϕ_1 (ϕ_2 has the opposite sign of ϕ_1), so the plot region is chosen to cover exactly a period of ϕ_1. Note that T_0 and T_1
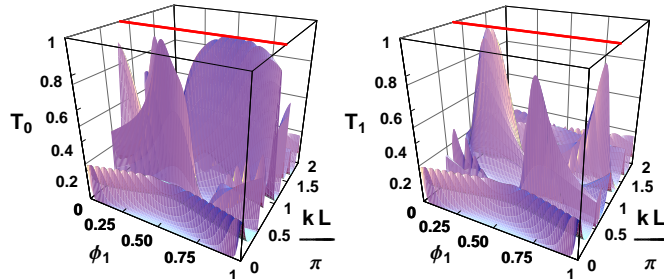
Figure 3.2: Transmission probabilities from the **0**-rail of the input to the **0**-rail (left panel) and **1**-rail (right panel) of the output. $\phi_1 * \phi_2 \leqslant 0, |\phi_1| = |\phi_2|$, $\log_2(k_g/k) = 2.275$. The red line (gray line) in top plane is drawn for $kL/\pi = 0.839$.

at $kL/\pi \simeq 0.839$ attain their maximum for different ϕ_1. This signals an opportunity to change the functionality of the quantum gate dynamically by tuning the magnetic flux.

Using the AB quantum gates we can control directly the phase of the electronic wave function. Increasing the phase ϕ_1 by 1 changes the arguments of the matrix elements T_{11}, T_{12}, T_{21}, T_{22} by $-\frac{1}{4}\pi$, $-\frac{1}{8}\pi$, $-\frac{1}{8}\pi$, 2π, without affecting their modulus. Similarly, increasing the phase ϕ_2 by 1 changes these arguments by 2π, $\frac{1}{8}\pi$, $\frac{1}{8}\pi$, $\frac{1}{4}\pi$ respectively. Such phase relationship holds for all k_g/k. Therefore, with a proper choice of kL/π and k_gL/π, one can obtain a set of quantum gates of different functionality simply by varying ϕ_1 and ϕ_2 through the action of the cantilevers. A set of elementary quantum gates, including the identity gate (**I**), Pauli-Z gate (σ_z), Pauli-X gate (σ_x), and the $\pi/8$ gate (T) is at our disposal. It should be noted that the AB quantum gates constructed in this way can only be symmetric. Asymmetric gates are achieved by connecting two or more gates in series. Varying kL/π, however,

Figure 3.3: Minimum error rate for the H and σ_x gate (dotted and solid line resp.). The horizontal dashed line stands for $\epsilon_{th} = 10^{-4}$.

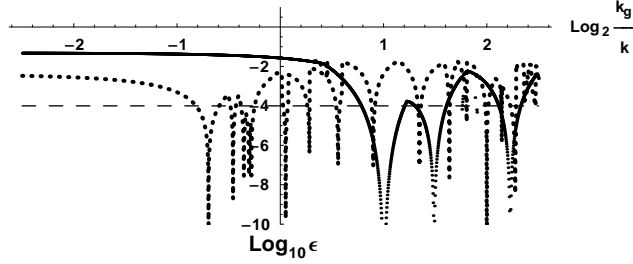we have also the Hadamard gate (H). By the H-gate and T-gate we can approximate any individual operation to arbitrary accuracy [46]. We list the AB quantum gates and the corresponding working points in Table 3.1 for $\log_2(k_g/k) = 2.275$.

In order to compare the error-prone (non-unitary) $\mathbf{T}$-gates with ideal error-free (unitary) gates ($\mathbf{U}$), we also present in the table estimates of the gate's error rate ϵ, which is defined as $\epsilon = 1 - F$, where $F = \left| \text{Tr}\left(TU^\dagger\right) \right| \Big/ \text{Tr}\left(UU^\dagger\right)$ is the gate fidelity [48]. Also, we take $\epsilon_{th} = 10^{-4}$ as a rough estimate of the threshold for quantum computation, below which an arbitrarily large computation can be performed efficiently [46]. Clearly, the proposed AB quantum gates demonstrate error rate below ϵ_{th}, which ensures the scalability of the architecture. Moreover, due to the periodical behavior of the AB quantum gates described above, we claim that the optimal operating points $(kL/\pi, k_gL/\pi, \phi_1, \phi_2)$ for a particular functionality can always be found by tuning and a very high fidelity can be achieved. Figure 3.3 shows an example of the behavior of the minimal error rate ε for σ_x and H gates to different k_g/k, when ϕ_1 and kL/π are varied over the plot region in Fig. 3.2. For several k_g/k the minimal error rates of both gates are beyond ϵ_{th}. The possibility to choose and tune the gate dynamically makes our architecture

31

Table 3.1: Error rate for the set of AB quantum gates. The second column defines the dynamic working points for the gates, $\log_2(k_g/k) = 2.275$.

Gate	I	σ_z	σ_x	T	H
$\log_{10} \epsilon$	-5.810	-5.810	-5.179	-5.810	-8.442
kL/π	0.839	0.839	0.839	0.839	1.219
ϕ_1	0.748	0.748	0.252	0.748	0.933
ϕ_2	3.252	-0.748	-0.252	0.252	-4.933

particularly promising.

3.4   Implementation

The proposed architecture can be implemented using two dimensional electron gas structures and applying the split-gate techniques to define the pattern of 1D quantum wires. Within the dual rail representation for ballistic electron flying qubits, initialization and measurement of the qubit states can be done as was proposed in [38]. Nano-sized magnets can be electroplated on the sample [43]. Lithographic techniques enable us to make well-defined shapes and locations. The dynamic control of the AB quantum gates is realized by flipping the magnetization of the nano-magnets with read-write heads [43] (which is shown in Fig. 3.1 as a cantilever). As a result we can manipulate the phase of the electronic wave functions. Furthermore, different magnitudes of ϕ_1 and ϕ_2 are obtained by varying the size of the magnets and the rings, or by enclosing many magnets in a single ring. In addition, the application of the split-gate techniques to a two dimensional electron gas makes the values of kL/π and k_gL/π tunable. Variation of the voltage

applied to the gate changes the lateral confinement of the electrons in the quantum wires and modifies k and k_g. So, we can tune separately all of the four variables to choose the working point $(kL/\pi, k_gL/\pi, \phi_1, \phi_2)$ and to achieve the highest fidelity.

The approach proposed in ([38]) uses ballistic electrons. The functionality of the gates in that design is defined at the stage of fabricating the computer. This architecture will seriously suffer from any fabrication defect because defects cannot be compensated afterwards. In contrast, the dynamic controllability in our proposition implies that the functionality of each gate can be re-defined after fabrication and even during operation. For instance one can dynamically re-assign a H-gate into a T-gate during the calculation process. Since it is possible to make a hybridization of quantum computers and classical computers in solid state circuits, a classical computer are used to operate the read-write head. Without this dynamic re-programmability the architecture can only serve as special purpose quantum circuits but not as quantum computers for general purposes. We emphasize that the above advantages are entirely due to the universality of the AB quantum gates – multi-functionality is achieved by changing through k and k_g and the enclosed magnetic fluxes. The utilization of a magnetic field, rather than an electric field like in [38], has other benefits: low power, insensitivity to noise, and less astray field.

3.5 Two-dimensional calculation using the lattice Green's function method

In the previous sections we have demonstrated good gate fidelity within an one-dimensional calculation. The applicability of such results, however, is

not clear for the following reasons. At each intersection, to connect the wave functions in different segments of quantum wires the Griffith [35] boundary conditions are imposed, which treat each segment as simple straight line without taking its geometry into consideration. Taking the geometry of quantum wires into account, we expect the transmission through an intersection maximizes only when the incident energy of electrons can couple to the quasi-bound states of the intersection. The transmission probability depends on incident energy complicatedly while that does not depend on incident energy if the Griffith boundary conditions are imposed. On the other hand, the construction of the σ_z and T gates in our architecture relies on how the phases of the transmission amplitudes increase with the magnetic flux. And the phase dependence is determined by the relative position of the incoming and outgoing leads along the ring. In real situation the leads and the arms of the rings have non-negligible width. Can we still establish a perfect phase property when the width effect is taken into account? If not, are we able to construct such gates like σ_z and T gates which require the phase-shifting property of the transmission amplitudes?

We perform a two-dimensional calculation based on the lattice Green's function method [41] to address the above questions. This method is suitable for our use because of its ability to calculate the transmission property for an arbitrarily shaped conductor. Another appealing feature of this method is that some types of magnetic fields may be incorporated quite simply into the formalism, and therefore it is well suited to study various effects of magnetotransport [41]. Moreover, we can obtain the Green's function recursively and then extract the scattering matrix elements from the Green's function as in [42]. The discretized mesh used in our calculation is shown in Fig. 3.4, and the single particle Green's function is solved on this mesh under the
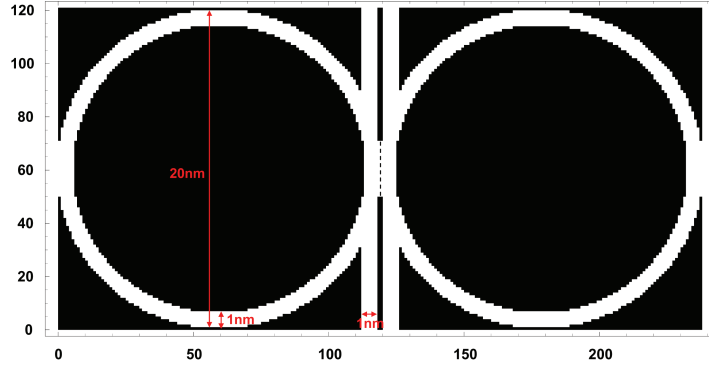
Figure 3.4: Actually simulated meshes in our calculation. The numbers along the axes are the index of the mesh. In this calculation 121×238 meshes are included. Red arrows indicating the relevant length of this system. The dashed line in the center separates the left half region and the right half one, across it the magnetic field is taken to be abruptly different. The effective mass of the electron is $0.09\ m_0$.

effective mass approximation. We have made an infinite barrier approximation, that is, the potential energy in the light region is set to be zero and that in the dark region is set to be infinite. The straight light segments in the center connect respectively to the semi-infinite incoming and outgoing leads, in which the magnetic field is assumed to be not present. However, at actually simulated mesh shown here the magnetic field is present, and is taken to be abruptly different in the left half region and the right half region (separated in the figure by a dashed line).

In a realistic two-dimensional calculation the quantum waveguides are not singlemoded. We define the logic state of the qubit as the presence of a single electron in the first transverse mode of a rail, and we restrict the incident energy in the range between the first and second transverse mode so as to minimize the error due to leakage to other transverse modes. The
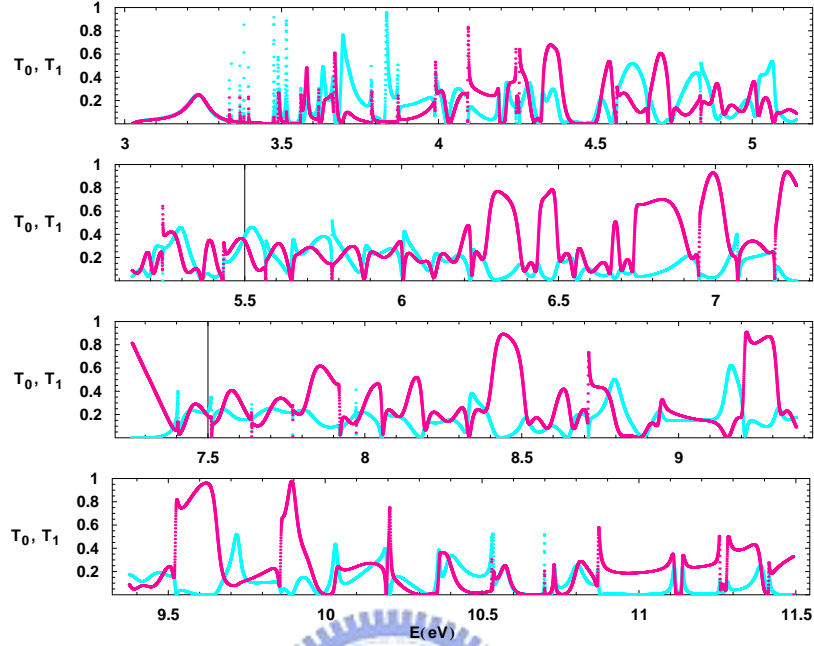
Figure 3.5: Transmission probabilities from the **0**-rail of the input to the **0**-rail (left panel) and **1**-rail (right panel) of the output at a zero magnetic field. The plot energy range is between the first and second transverse mode, 3.02eV and 11.49eV in this system. The light and dark line correspond to T_0 and T_1, respectively.

probabilities of transmission T_0 and T_1 ($\mathrm{T}_0 = |T_{11}|^2$, $\mathrm{T}_1 = |T_{12}|^2$) at a zero magnetic field are shown in Fig. 3.6 in the energy range between the first and second transverse mode. The zero energy point is set at the conduction band edge. The incorporation of the geometry of the intersection greatly complicates the energy response of the coupled ring system, as contrasted to the one-dimensional situation where T_0 and T_1 are periodic to kL/π. Another notable feature of this system is that the incident electron from the input **0**-rail can better couple to the output **1**-rail rather than to the output **0**-rail (we will be more precise to this claim later).
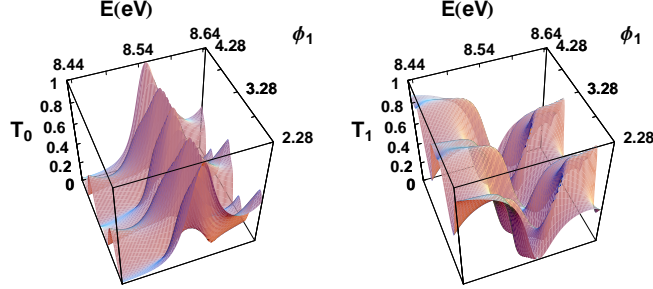
Figure 3.6: Transmission probabilities from the **0-**rail of the input to the **0-**rail (left panel) and **1-**rail (right panel) of the output. $\phi_1 * \phi_2 \leqslant 0, |\phi_1| = |\phi_2|$.

In Fig. 3.6 we calculate T_0 and T_1 with respect to the incident electron energy and the normalized magnetic flux ϕ. Here the normalized flux ϕ is defined by $\phi_i = \Phi_i/\Phi_0$, where Φ_i is the average of the magnetic flux enclosed by the outer or inner circle, through the left ($i = 1$) or right ($i = 2$) ring. In the two unit of ϕ_1 of the plot region shown here, the transmission probabilities are almost periodic to ϕ_1 (ϕ_2 has the opposite sign of ϕ_1). Having the ratio of wire width to ring radius as $\frac{1}{10}$, this system well retains the periodic oscillation of the transmission probability with respect to the enclosed magnetic flux.

To observe how the non-negligible widths of the quantum wires affects the phase property of T_{11} and T_{12}, the phase relationship at $E = 8.548(eV)$ is illustrated Fig. in 3.7 to ϕ_1 (ϕ_2 has the opposite sign of ϕ_1). The argument of T_{11} increases about 0.103π (or $\frac{1}{9.749}\pi$) at a unit of ϕ_1, while that of T_{12} increases half as fast. Although in this two-dimensional system we tried to keep our original design (i.e., we deploy the two leads along the ring at a distance of $\frac{2}{16}$ ring circumference), the increment of the arguments is different from what we have designed in the one-dimensional case. Also, the increment of the arguments at a unit of ϕ_1 is no longer exactly the same at different
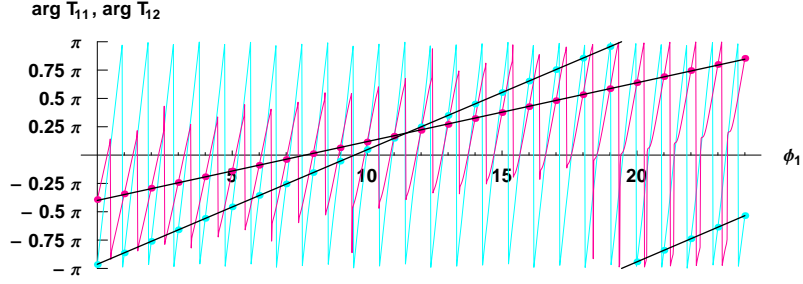
37

Figure 3.7: Arguments of T_{11} and T_{12} at $E = 8.548(eV)$ (the light and dark line resp.). The dots mark the increment of the arguments at each unit of ϕ_1 and the straight lines are linear fittings of the increment.

E and ϕ_1, but in the figure shown the increment varies less than 1.5% from a linear extrapolation. Since the increment of the arguments is not even rational numbers, it is not apparent here whether the phase property of this two-dimensional system could facilitate the construction of the σ_z and T gates. From the working points shown in Table 3.2, however, we indeed see the working points of the σ_z and T gates deviate from the working point of the I gate only by almost integer units of ϕ_1 and ϕ_2. How could non-rational increment of the arguments adds up to a phase difference of $\pi/4$ or π between T_{11} and T_{12}? It may be explained as the following. Not only does the increment of the arguments increases linearly at each integer point of ϕ_1, the arguments themselves increase linearly in between integer points of ϕ_1. Note that the former claim holds at other energies but the latter does not. So the working points of the σ_z and T gates will not deviate very far from that of the I gate by exactly integer shifts of ϕ_1 and ϕ_2, and the fidelity of the I gate can be retained or even improved for the two gates. Another interesting thing to note is that the σ_x gate has a fidelity even higher than that of the I gate and reaches the threshold fidelity of quantum computation. By applying a gate voltage to the central region as what we have done in the

38

Table 3.2: Error rate for the set of AB quantum gates in the two-dimensional calculation. The second column defines the dynamic working points for the gates.

$Gate$	I	σ_z	σ_x	T	H
$\log_{10} \epsilon$	-3.202	-3.197	-4.157	-3.453	-2.529
$E(eV)$	8.548	8.548	6.896	8.548	9.476
ϕ_1	3.282	7.280	-0.528	2.268	7.261
ϕ_2	-3.282	2.718	0.528	-4.294	4.605

one-dimensional calculation, we expect other quantum gates could reach the threshold fidelity as well.

3.6 Conclusion

In conclusion, we proposed and analyzed an architecture for quantum computation with ballistic electrons: coupled ballistic Aharonov-Bohm quantum gates. On the one hand, such quantum gates can be tuned, controlled and reprogrammed dynamically. On the other hand, in properly selected operation regimes, the fidelity of the gates can attain about 0.99999.

We would like to point out that our architecture can be used as a starting point for the implementation of dynamically reprogrammable quantum computers based on electrons as qubits and coupled quantum rings as quantum gates. On the other hand, the main idea to use an external magnetic flux as a dynamic factor to reprogram quantum computers during the calculation process is more general and potentially very rich. The rapid progress in the fabrication of quantum magnetic disks and the already elaborated

high quality two dimensional electron systems make us claim that quantum computation with the ballistic Aharonov-Bohm quantum gates is not only promising but also feasible in the near future.

Chapter 4

Conclusions

In conclusion, we investigated two systems which could be useful in implementing quantum computing with mobile qubits. In chapter 2, we present the numerical results of the tunneling time through a realistic InGaAs/InAlAs/InGaAs resonant symmetric structure with the Dresselhaus spin-orbit coupling. The results indicate that the Dresselhaus spin-orbit coupling separates the time-dependent response of differently spin-polarized tunneling electrons. The large and tunable ratio of the tunneling times provides a possible way to construct a dynamic spin filter, which is a basic element in spintronics as well as quantum computing with mobile spin qubits. In chapter 3, we proposed and analyzed an architecture for quantum computing with mobile charge qubits: coupled ballistic Aharonov-Bohm quantum gates. Such quantum gates can be tuned, controlled and reprogrammed dynamically. In properly selected operation regimes, the gates demonstrate an excellent fidelity of 0.99999. The central idea to use an external magnetic flux as a dynamic factor to reprogram quantum computers during the calculation process is potentially very rich. We hope our research could be useful and intriguing to the wide community of quantum computation and information.

Bibliography

[1] R. P. Feynman, Int. J. of Theor. Phys., **21**, 467(1982).

[2] D. Deutsch, Proc. R. Soc. Lond. A, **400**, 97(1985).

[3] P. W. Shor, Algorithms for quantum computation:discrete logarithms and factoring. *Proc. of 35th Annual Sumposium on Fundamentals of Computer Science* (IEEE press, Los Alamitos, CA, 1994).

[4] L. Grover, *Proc. of 28th Annual ACM Sumposium on on the Theory of Computation*, pages 212-219 (ACM press, New York, 1996).

[5] S. L. Braunstein and H. K. Lo(Eds.), *Scalable Quantum Computers* (WILEY-VCH, Berlin, 2001).

[6] D. P. DiVincenzo, G. Burkard, D. Loss and E. Sukhorukov, in *Quantum Mesoscopic Phenomena and Mesoscopic Devices in Microelectronics*, eds. I. O. Kulik and R. Ellialtoglu (NATO ASI, Turkey, June 13-25, 1999).

[7] A. E. Popescu and R. Ionicioiu, Phys. Rev. B **69**, 245422 (2004).

[8] S. Datta and B. Das, Appl. Phys. Lett. **89**, 665(1990).

[9] G. Schmidt, D. Ferrand, L.W. Molenkamp, A.T. Filip, and J. van Wees, Phys. Rev. B **62**, R4790 (2000).

[10] P. R. Hammar, B. R. Bennett, M. J. Yang and M. Johnson, Phys. Rev. Lett. **83**, 203(1999); S. Gardelis, C. G. Smith, C. H. W. Barnes, E. H. Linfield, and D. A. Ritchie, Phys. Rev. B **60**, 7764(1999); D. D. Awschalom, D. Loss, and N. Samarth (Eds), *Semiconductor Spintronics and Quantum Computation* (Springer, Berlin, 2002).

[11] Yu. A. Bychkov and E. I. Rashba, J. Phys. C **17**, 6039 (1984).

[12] G. Dresselhaus, Phys. Rev. **100**, 580 (1955).

[13] E. A. de Andrada e Silva, Phys. Rev. B **46**, 1921 (1992); E. A. de Andrada e Silva, and G. C. La Rocca, Phys. Rev. B **50**, 8523 (1994).

[14] A. Voskoboynikov, S.S. Liu, and C.P. Lee, Phys. Rev. B **59**, 12 514 (1999).

[15] E. A. de Andrada e Silva, and G. C. La Rocca, Phys. Rev. B **59**, 15583 (1999).

[16] A. Voskoboynikov, S.S. Liu, and C.P. Lee, J. Appl. Phys. **87**, 387 (2000).

[17] T. Koga, J. Nita, H. Takayanagi, and S. Datta, Phys. Rev. Lett. **88**, 126601 (2002).

[18] Z.-Y. Ting, D. X. Cartoixá, D. H. Chow, J. S. Moon, D. L. Smith, T. C. McGill, and J. N. Schulman, Proc. IEEE, **91**, 741 (2003).

[19] J. S. Moon, D. H. Chow, J. N. Schulman, P. Deelman, J. J. Zinck, and D. Z.-Y. Ting, Appl. Phys. Lett. **85**, 678 (2004).

[20] V. I. Perel', S. A. Tarasenko, I. N. Yassievich, S. D. Ganichev, V. V. Bel'kov, and W. Prettl, Phys. Rev. B **67**, 201304 (2003).

[21] D. Z.-Y. Ting and X. Cartoixà, Phys. Rev. B **68**, 235320 (2003).

[22] D. Bohm, *Quantum Theory*, Prentice-Hall, New York, 1951; M. Buttiker, R. Landauer, Phys. Rev. Lett. **49**, 1739 (1982); D. Dragonman, M. Dragonman, IEEE J. Quantum Electron. **32**, 1932 (1996); G. Garcia-Calderon, A. Rubio, Phys. Rev. B **55**, 3361 (1997); J. U. Kim, H. H. Lee, J. Appl. Phys. **84**, 907 (1998).

[23] O. Voskoboynikov, S. S. Liu, and C. P. Lee, Solid State Commun. **155**, 477 (2000).

[24] G. Bastard, *Wave Mechanics Applied to Semiconductor Heterostructures* (Les Edition de Physique, Les Ulis, 1990).

[25] E. O. Kane, *Tunneling Phenomenon in Solids* (Plenum, New York, 1969).

[26] S. Sen, F. Capasso, A. L. Hutchinson, and A. Y. Cho, Electron. Lett. **23**, 1229 (1988).

[27] J. H. Davies, *The Physics of Low-dimensional Semiconductors: An Introduction* (Cambridge University Press, Cambridge, 1998).

[28] R. Eppenga, and M. F. H. Schuurmans, Phys. Rev. B **37**, 10923 (1988).

[29] J. Singh, *Electronics and Optoelectronic Properties of Semiconductor Structures*(Cambridge University Press, Cambridge, 2003).

[30] P. Singha Deo and A. M. Jayannavar, Phys. Rev. B **50**, 11629(1994).

[31] Han-Chun Wu, Yong Guo, Xin-Yi Chen and Bing-Lin Gu, Phys. Rev. B **68**, 125330(2003).

[32] C. H. Wu and Diwakar Ramamurthy, Phys. Rev. B **65**, 075313(2002).

[33] A. M. Jayannavar and P. Singha Deo, Phys. Rev. B **49**, 13685(1994).

[34] D. M. Pozar, *Microwave Engineering*, 3 ed.(Wiley, US, 2004).

[35] J. S. Griffith, Tran. Faraday Soc. **49**, 345(1953).

[36] A. Bertoni, P. Bordone, R. Brunetti, C. Jacoboni, and S. Reggiani, Phys. Rev. Lett., **84**, 5912(2000).

[37] J. Harris, R. Akis, and D. K. Ferry, Appl. Phys. Lett. **79**, 2214(2001).

[38] R. Ionicioiu, G. Amaratunga and F. Udrea, Int. J. of Mod. Phys. B, **15**, 125(2001).

[39] Y. Aharonov and D. Bohm, Phys. Rev. **115**, 485(1959).

[40] S. Datta et. el., Phys. Rev. Lett. **55**, 2344(1985).

[41] D. K. Ferry and S. M. Goodnick, *Transport in nanostructures*(Cambridge University Press, Cambridge, 1997); S. Datta, *Electronic transport in mesoscopic systems*(Cambridge University Press, Cambridge, 1995);

[42] T. Ando, Phys. Rev. B **44**, 8017(1991).

[43] S. Y. Chou, M. S. Wei, P. R. Krauss, and P. B. Fischer, J. Appl. Phys., **76**, 6673(1994).

[44] I. Chuang and Y. Yamamoto, Phys. Rev. A **52**, 3489(1995).

[45] C. H. Wu and Diwakar Ramamurthy, Phys. Rev. B **65**, 075313(2002).

[46] M. A. Nielsen and I. L. Chuang, *Quantum Computation and Quantum Information*(Cambridge University Press, Cambridge, 2000).

[47] J. Xia, Phys. Rev. B **45**, 3593(1992).

[48] D. Mc Hugh and J. Twamly, Phys. Rev. A **71**, 012327 (2005).